Macromolecular Rapid Communication
www.mrc-journal.de

2D Chiral Stripe Nanopatterns Self-Assembled from Rod-Coil Block Copolymers on Microstripes

Zhengmin Tang, Zhanwen Xu, Chunhua Cai, Jiaping Lin,* Yuan Yao, Chunming Yang, and Xiaohui Tian*

Chiral nanoarchitectures usually possess unique and intriguing properties. However, the construction of 2D chiral nanopatterns through polymer self-assembly is a challenge. Reported herein is the formation of chiral stripe nanopatterns through surface self-assembly of polypeptide-based rod-coil block copolymers on microstripes. The nanostripes align oblique to the boundary of the microstripes, resulting in the chirality of the nanopatterns. The chirality of the nanopatterns is closely related to the width of the microstripes, i.e., a narrower width results in higher chirality. Besides, the chiral sense of the nanopatterns can be regulated by the chirality of the polypeptide blocks. This work demonstrates the transmission of chirality from polymer to nanoarchitecture on a confined surface, which can guide the preparation of nanopatterns with tuned chiral features.

Chiral structures are ubiquitous in nature from the molecular to the macroscopic level.[1] For example, the rotation direction of mollusk shells is right-handed, and many vine plants also tend to grow along the right-handed direction. Basically, such macroscopic chiral structures are generated in the presence of chiral biomolecules. Inspired by nature, chiral molecules and other chiral motifs have been used as building blocks to construct multifarious chiral supramolecular assemblies.[2–4] Among the chiral assembly structures, 2D chiral nanoarchitectures have recently attracted increasing attention.[5–9] Due to their special topological features and intriguing functions, 2D chiral nanostructures show broad potential applications in the fields of catalysis, sensors, protein adsorption, and cell adhesion.[8,10–13]

Z. Tang, Dr. Z. Xu, Prof. C. Cai, Prof. J. Lin, Prof. Y. Yao, Prof. X. Tian
Shanghai Key Laboratory of Advanced Polymeric Materials
Key Laboratory for Ultrafine Materials of Ministry of Education
School of Materials Science and Engineering
East China University of Science and Technology
Shanghai 200237, China
E-mail: caichunhua@ecust.edu.cn; jlin@ecust.edu.cn
Dr. C. Yang
Shanghai Synchrotron Radiation Facility
Shanghai Advanced Research Institute
Chinese Academy of Sciences
Shanghai 201204, China
The ORCID identification number(s) for the author(s) of this article can be found under https://doi.org/10.1002/marc.202000349.

DOI: 10.1002/marc.202000349

Self-assembly of block copolymers provides an effective way to produce ordered nanostructures.[14,15] To prepare chiral assembly nanostructures, confinement is usually necessary. When self-assembly occurs in a confined space, such as spheres, cylinders (nanopores), and circles, the block copolymers are able to form diverse chiral nanostructures, including helices, helical balls, and spirals.[16–23] However, there are very limited examples to date regarding the self-assembly of block copolymers into 2D well-defined chiral nanoarchitectures on a confined substrate. Recent works have shown that well-ordered nanopatterns of block copolymers can be constructed by introducing chemical or topological confinement to a substrate,[15,24,25] but these nanopatterns rarely possess chirality characteristics. It is still a challenge to create 2D chiral nanoarchitectures from synthetic polymer systems, especially large nanopatterns with controllable chirality.

Herein, we report the formation of chiral stripe nanopatterns on microstripes through surface self-assembly of poly(γ-benzyl-L-glutamate)-*block*-poly(ethylene glycol) (PBLG-*b*-PEG) block copolymers in which PBLG is a rigid helical polypeptide block. The nanopatterns possess clockwise chirality, which is closely related to the confinement effect of the microstripes and the chirality of the polypeptide blocks.

The typical experimental procedure involves two consecutive assembly steps, as illustrated in **Scheme 1**. First (**Step 1**), polystyrene (PS) microstripes were prepared via controlled evaporative self-assembly of PS toluene solution confined in a "cylinder-on-Si" geometry.[26,27] After heat treatment (temperature: 160 °C) and extensive rinsing with toluene, alternating hydrophobic ultrathin PS microstripes formed on the Si substrate. The PS microstripes were irreversibly adsorbed on the substrate.[28,29] In **Step 2**, the PS microstripes on the substrate were used as templates to direct the surface self-assembly of PBLG-*b*-PEG (temperature: 20 °C).[23,30] Typically, PBLG-*b*-PEG copolymers were dissolved in a mixed solvent of tetrahydrofuran (THF) and *N,N*′-dimethylformamide (DMF) (THF/DMF, 7/3 v/v), and the substrate was immersed in the polymer solution with the PS microstripes facing up. Then, water, a selective solvent for PEG blocks was added. The addition of water gives rise to the adsorption and assembly of PBLG-*b*-PEG on the hydrophobic PS microstripes. By fluorescently labelling the

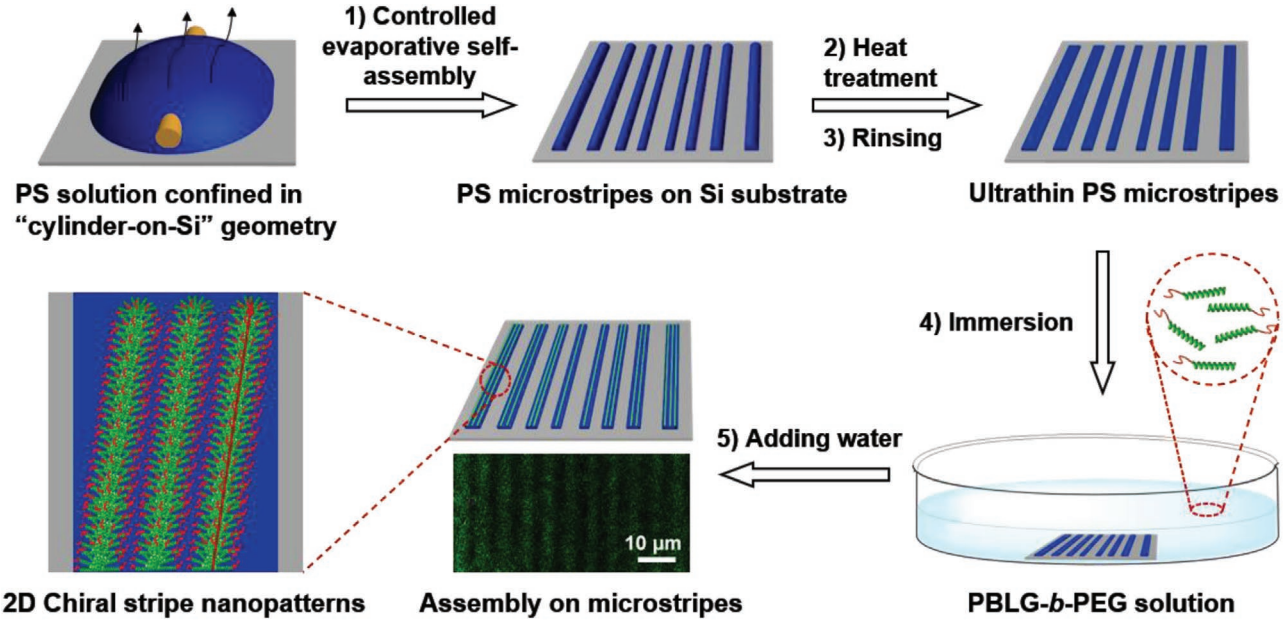

Scheme 1. Schematic illustration of the formation of chiral stripe nanopatterns on microstripes. Upper panel: PS microstripes were prepared via controlled evaporative self-assembly of PS toluene solution confined in a "cylinder-on-Si" geometry. Lower panel: the PS microstripes on the substrate were used to direct the surface self-assembly of PBLG-*b*-PEG. The addition of water induces the assembly of PBLG-*b*-PEG on the hydrophobic PS microstripes, forming well-ordered chiral stripe nanopatterns. The image consisting of alternating green and dark microstripes was captured by confocal laser scanning microscopy.

PBLG block of the copolymer, alternating light (green, block copolymer domain) and dark (blank Si domain) microstripes were observed in the confocal laser scanning microscopy image (see Scheme 1, bottom middle panel), which proved the deposition of PBLG-*b*-PEG on microstripes. In these microstripes, the block copolymers form well-ordered stripe nanopatterns (**Scheme 1**, bottom left panel; see the discussion below).

Figure 1a,b shows the representative 3D atomic force microscopy (AFM) image and the corresponding height profile of the ultrathin PS microstripes formed on the Si substrate. The PS microstripes have a nearly smooth surface and a height of ≈9 nm. In addition, the width of the PS microstripes ranges from ≈1.1 to ≈2.5 μm in gradient (see Figure S2 in the Supporting Information). Figure 1c shows the AFM image of the stripe nanopatterns self-assembled from $PBLG_{12k}$-*b*-PEG_{5k} (the subscripts denote the number-average molecular weight, M_n, for each block) on the PS microstripes. By comparing the height of the original PS microstripes (≈9 nm) and that of the films (≈15 nm, Figure 1d), the average height of the nanopatterns was determined to be ≈6 nm. The stripe nanopatterns were regular with a periodicity of ≈50 nm. The ordered stripe nanopatterns covered the entire area of the PS microstripes, which can be several millimeters in length. From grazing-incidence small-angle X-ray scattering (GISAXS) testing, as shown in Figure 1e, apparent scattering spots at the q_y value of 0.129 nm^{-1} were observed, which suggests the in-plane order of the stripe nanopatterns with a periodicity of 48.8 nm. The GISAXS result is consistent with the AFM measurements.

Figure 1f–h shows the AFM phase images of the stripe nanopatterns self-assembled from $PBLG_{12k}$-*b*-PEG_{5k} on PS microstripes with widths of 1.1, 1.5, and 2.5 μm. As indicated by the red lines in Figure 1f–h, the block copolymer nanostripes are well-ordered and align obliquely on the PS microstripes. In the fast Fourier transform (FFT) images (the insets of Figure 1f–h), the connection lines of the scattering spots are nonhorizontal, suggesting that the nanostripes are not parallel to the PS microstripes. By combining the AFM observations and FFT results, a clockwise chiral characteristic of these asymmetric nanopatterns is determined. To give a clear description of the orientation of block copolymer nanostripes, we define an orientation angle (θ) between the long axis of nanostripes and the boundary of the PS microstripes (see the inset of Figure 1i). Here, when $\theta = 0°$, the nanostripes adopt a parallel alignment relative to the boundary of PS microstripe, displaying no chirality. A diagram referring to the average θ (measured from FFT images) versus the width of the PS microstripe is plotted in Figure 1i. As can be seen, all the θ values are positive, indicating that the chirality of all these nanopatterns is clockwise. The average θ decreases with increasing width of the PS microstripe, suggesting that the nanostripes are less inclined to tilt toward the right boundary of the microstripe when the width of PS microstripe is broader. Therefore, it is deduced that when self-assembling on a wide PS microstripe, the block copolymers should form stripe nanopatterns with no chirality. Such a perspective has been confirmed by a control experiment using a wide PS microstripe and a millimeter-scale PS film as the substrate (Figure S3, Supporting Information). These results suggest that the chirality expression of nanopatterns is related to the confinement of the PS microstripes.

The inner structures of the block copolymer nanostripes were then analyzed. The AFM images reveal that the width of the nanostripes is ≈22 nm and the height is ≈6 nm. Considering the geometrical structure of the nanostripes and the assembly

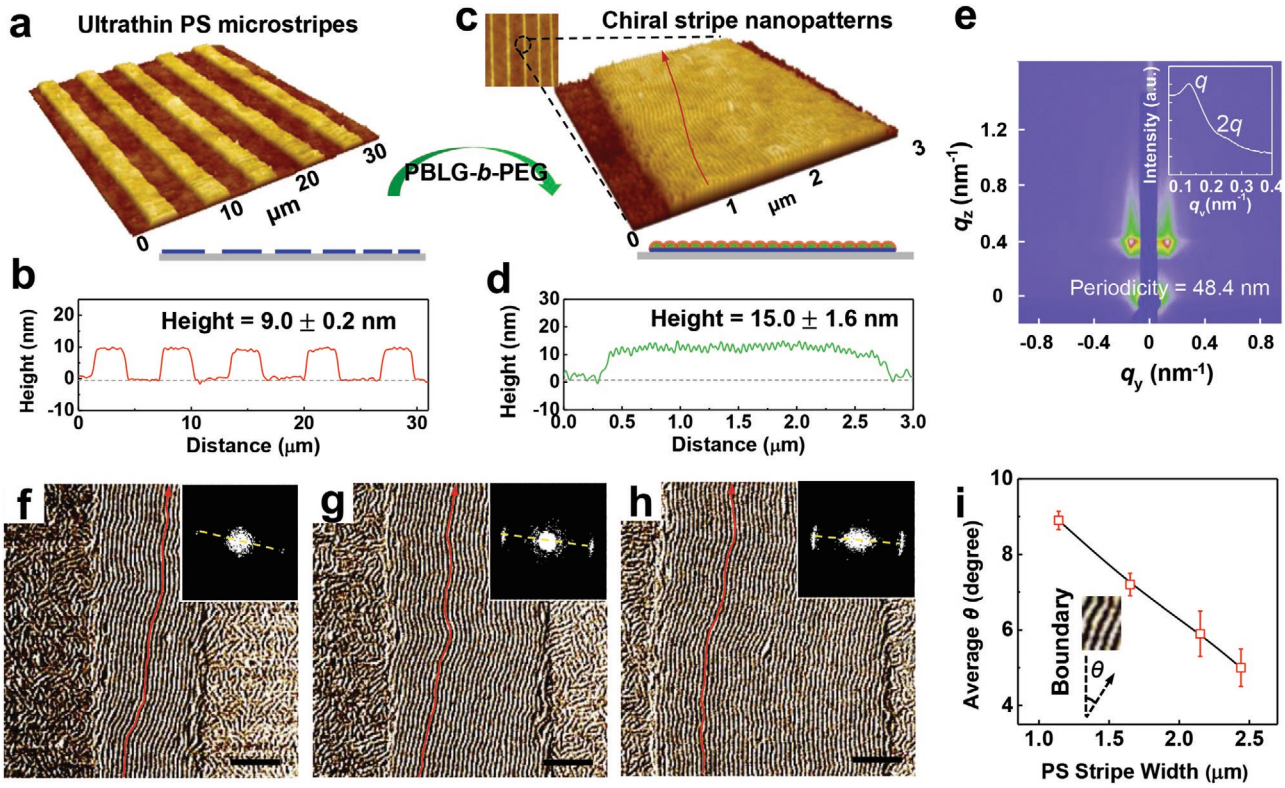

Figure 1. a,c) 3D AFM images and b,d) the corresponding height profiles of the ultrathin PS microstripes and the stripe nanopatterns, respectively. The bottom right insets of (a) and (c) show the side-view cartoon of PS microstripes and the nanopatterns on a microstripe, respectively. e) 2D GISAXS pattern of the film. The inset shows the 1D profile of the pattern. f–h) Representative AFM phase images of the well-ordered stripe nanopatterns self-assembled from PBLG$_{12k}$-*b*-PEG$_{5k}$ on the PS microstripes with widths of 1.1, 1.5, and 2.5 μm, respectively. The red lines indicate the oblique orientation of nanostripes with respect to the right boundary of the PS microstripe. The insets show the fast Fourier transform (FFT) of the images in which the yellow dashed lines connect the bright scattering spots. Scale bars: 500 nm. i) The dependence of the average θ on the width of the PS microstripe. The inset shows the definition of the angle θ. The values of average θ were measured from FFT images.

mechanism of amphiphilic block copolymers in selective solvents, the inner structures of nanostripes could be assigned to surface micelles.[30,31] In the surface micelles, hydrophobic PBLG blocks form the core, and hydrophilic PEG blocks form the corona. This assumption of structures was further verified by dissipative particle dynamics (DPD) simulations. In the DPD methods, PBLG$_{12k}$-*b*-PEG$_{5k}$ was mapped into R_6C_6 block copolymers, where the PBLG rod blocks and the PEG coil blocks are represented by R and C beads, respectively (**Figure 2**a). To model the PS microstripes on the substrate, a coarse-grained planar substrate covered by homopolymer microstripe (P) was constructed, as shown in Figure 2b. The selective solvents were denoted by S beads (not shown). To model the self-assembly of PBLG-*b*-PEG block copolymers on PS microstripes in the experiments, the interaction parameter between the rod blocks and the microstripes (a_{RP}) was set as 25. The interaction parameter between the hydrophobic rod blocks and the solvent (a_{RS}) was set as 70. More details about the model mapping and the parameter settings can be found in Section S2 in the Supporting Information. After the simulation system reached the equilibrium state, as seen in Figure 2c, stripe nanopatterns were formed on the surface of the microstripe. The cross-sectional image reveals that the nanostripes have a hemicylindrical micelle structure, where the hydrophobic rod blocks (R) form the core, and the hydrophilic coil chains (C) form the corona extending to the solution (Figure 2d). Furthermore, because of the rigidity of the R blocks, they tend to align in a head-to-head manner perpendicular to the long axis of the nanostripes (Figure 2e).[32–34] These simulations confirmed the assumption that the inner structure of the nanostripes is surface micelles formed by the PBLG-*b*-PEG block copolymers.

As revealed above, the stripe nanopatterns possess identical clockwise chirality in all the PS microstripe regions. This could be related to the chirality of helical polypeptide blocks.[4,22,35] To verify this assumption, we examined the self-assembly of PBDG$_{12k}$-*b*-PEG$_{5k}$ (PBDG: poly(γ-benzyl-$_D$-glutamate)) on PS microstripes. PBLG and PBDG are a pair of enantiomers that possess secondary structures (α-helix conformation) with opposite helical sense (Figure S4a, Supporting Information). As shown in **Figure 3**a, under similar experimental conditions, the PBDG$_{12k}$-*b*-PEG$_{5k}$ copolymers self-assembled into stripe nanopatterns with anticlockwise chirality (indicated by the blue line). Additionally, the chirality of nanopatterns can be regulated by mixing PBLG$_{12k}$-*b*-PEG$_{5k}$ and PBDG$_{12k}$-*b*-PEG$_{5k}$ copolymers in various mixing ratios. Figure 3b shows the plot of the average orientation angle θ of stripe nanopatterns as a function of the weight percentage of PBDG$_{12k}$-*b*-PEG$_{5k}$ in the mixtures. As can be seen, with increasing content of PBDG$_{12k}$-*b*-PEG$_{5k}$ in the

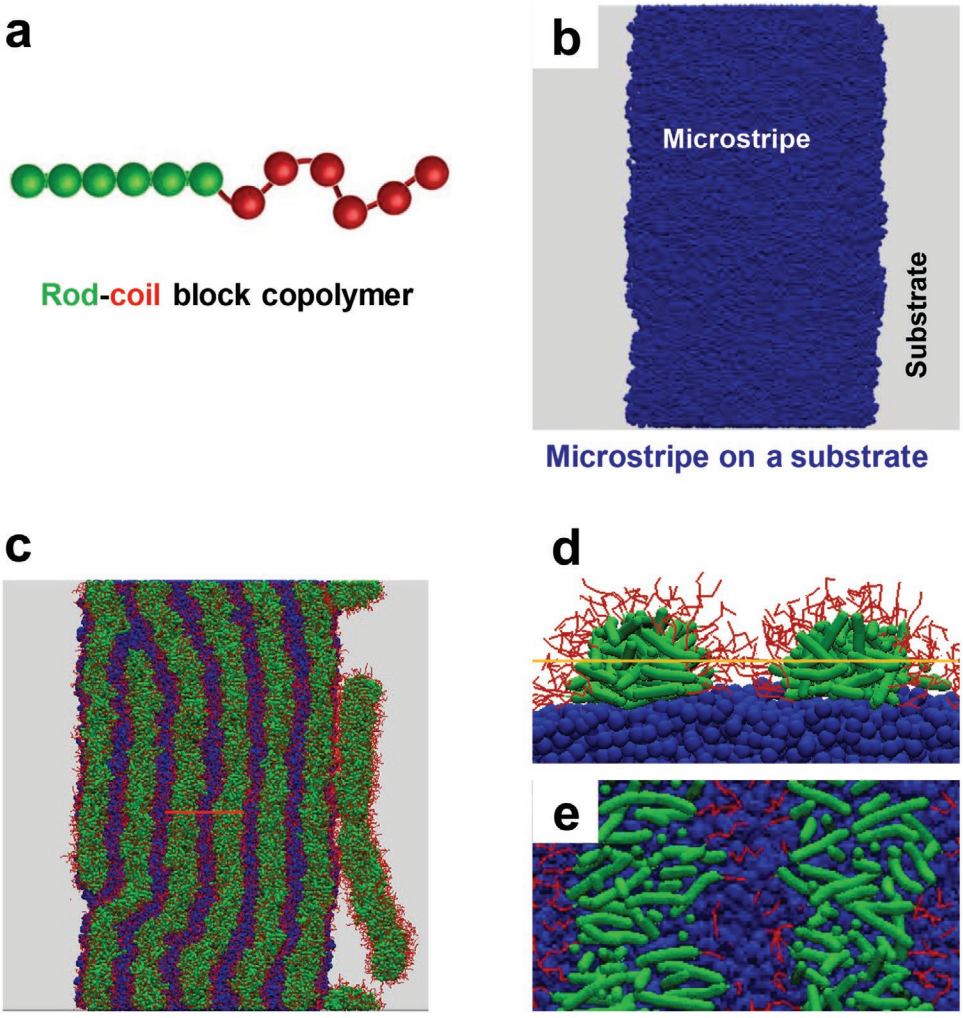

Figure 2. DPD model of a) the R_6C_6 rod-coil block copolymer, and b) the microstripe on a substrate. The rod and coil blocks and the microstripe are colored by green, red, and blue, respectively. c) Simulation prediction of the stripe nanopatterns formed on the microstripe. d) Cross-sectional image of the block copolymer nanostripes along the red line in panel (c). e) Cross-sectional image of the nanostripes along the yellow line in panel (d).

polymer mixtures, the angle θ gradually decreases and becomes nearly 0° when the $PBDG_{12k}$-*b*-PEG_{5k} content reaches ≈50 wt%, resulting in the formation of achiral stripe nanopatterns. Upon further increasing the content of $PBDG_{12k}$-*b*-PEG_{5k}, stripe nanopatterns with anticlockwise chirality are observed. These results demonstrate a chirality transmission process from the molecular chirality (helical backbone) of polypeptide blocks to nanopatterns on a confined surface.

To further explore how the PBLG-*b*-PEG copolymers assemble into chiral stripe nanopatterns on PS microstripes, we examined the dynamic process of the formation of nanopatterns by monitoring the morphological evolution on PS microstripes. In the experiments, self-assembling systems with various added water contents were incubated for more than 2 h to ensure that equilibrium structures were obtained. Then, the substrates were taken out from the solution, and the morphologies were observed from AFM. When the added water content was 9.1 vol%, as shown in **Figure 4**a, no characteristic morphology was observed on the surface of the microstripes. When the added water content was increased to 16.7 vol%, disordered structures were observed, suggesting the deposition of PBLG-*b*-PEG (Figure 4b). Upon further increasing the water content to 23.1 vol%, nanopatterns with local-ordered structures were formed (Figure 4c). Furthermore, the orientations of the nanostripes on both boundaries of the PS microstripes tilted toward the right side (indicated by dashed rectangles). Finally, when the added water content reached 28.6 vol%, well-ordered chiral nanopatterns were formed (Figure 4d). The critical water content for the formation of chiral structures on PS microstripes is determined to be ≈24.3 vol% (Figure S5, Supporting Information). These observations suggest that the formation of chiral stripe nanopatterns is a self-assembly process, including the adsorption of PBLG-*b*-PEG copolymers on PS microstripes and the subsequent structural reconstruction of copolymers into ordered nanopatterns. This disorder-to-order transition was accompanied by rearrangement of the rod-coil block copolymers to minimize the energetically unfavorable surface area between the hydrophobic PS/PBLG segments and solvents.[36] Additionally, due to the rigid nature of the PBLG blocks, the tendency for the ordered packing of rod blocks

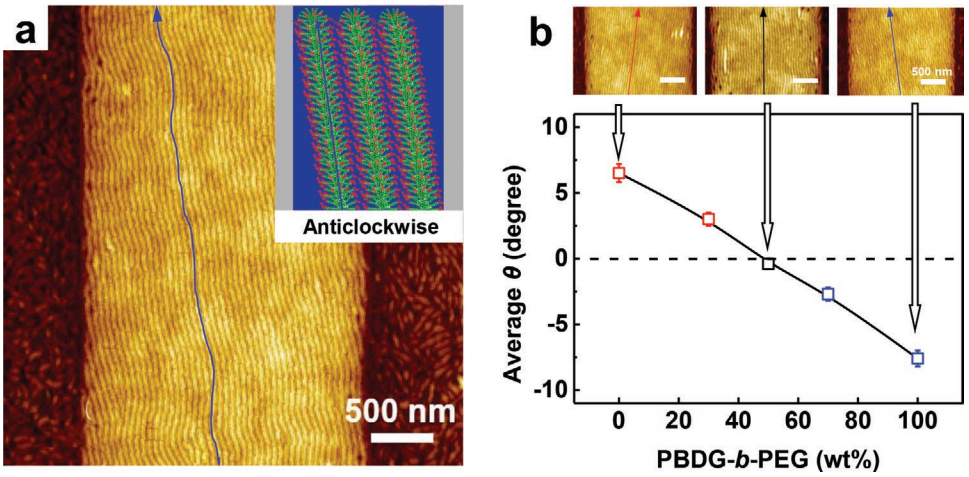

Figure 3. a) AFM topographic image of the stripe nanopatterns with anticlockwise chirality (oblique alignment relative to the left boundary of the PS microstripe, indicated by the blue line) self-assembled from $PBDG_{12k}$-*b*-PEG_{5k} copolymers on PS microstripes. The inset shows the cartoon of the anticlockwise chiral stripe nanopatterns. b) Dependence of the average angle θ of the stripe nanopatterns assembled on PS microstripes on the weight percentage of $PBDG_{12k}$-*b*-PEG_{5k}.

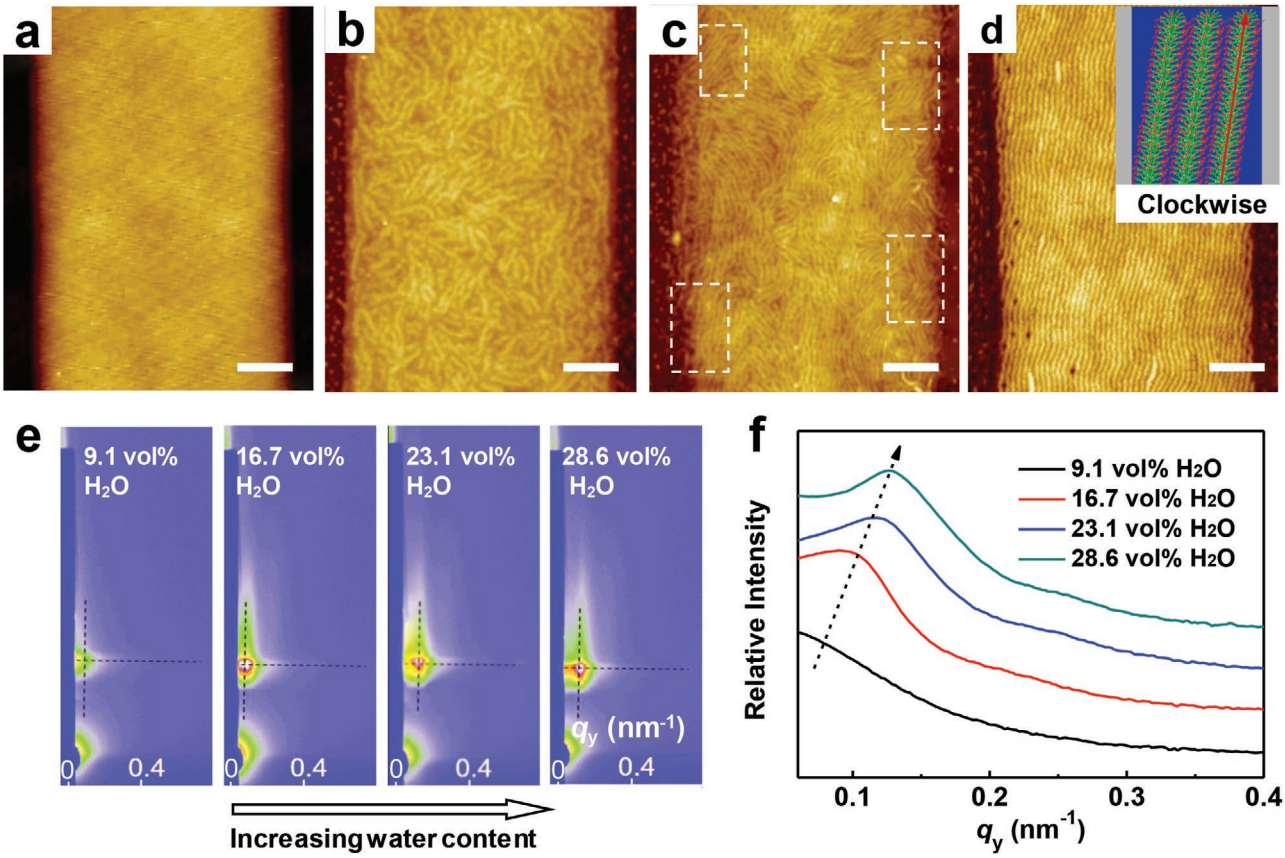

Figure 4. a–d) AFM topographic images of the morphological evolution process of the stripe nanopatterns on PS microstripes at various water contents of 9.1, 16.7, 23.1, and 28.6 vol%, respectively. The dashed rectangular regions in c mark the local stripe nanopatterns at the boundary of the PS microstripe. The inset of (d) shows the cartoon of the clockwise chiral stripe nanopatterns. Scale bars: 500 nm. e) 2D GISAXS pattern evolution for samples with increasing water content from 9.1 to 28.6 vol%. The cross of the black dashed lines in the patterns mark the scattering spots. f) Corresponding 1D profiles calculated from the GISAXS measurements. The dashed arrow indicates the shift of the scattering peaks.

could promote the formation of well-aligned nanostructures during self-assembly.[30,37]

GISAXS analysis was also used to trace the ordering process of nanopatterns. As shown in Figure 4e, the scattering intensity in the q_y direction became stronger with increasing water content, which indicates an increase in the in-plane order degree of stripe nanopatterns. Figure 4f shows the relative intensity profiles along the *y*-direction obtained from the GISAXS patterns. The main peaks of the curves shifted to a larger q_y value (from 0.103 to 0.127 nm^{-1}), corresponding to a decrease in the periodicity of the nanopatterns from 61.0 to 49.4 nm. In addition, the peaks became narrower, which suggests an increase in the ordering of the nanopatterns. Such GISAXS results demonstrate the disorder-to-order self-assembly process of the block copolymers on microstripes.

A possible mechanism underlying the formation of chiral stripe nanopatterns on PS microstripes is proposed in light of the above experimental and simulation results. The PBLG-*b*-PEG copolymers are well dissolved in the THF/DMF mixture. When water is added, the copolymers are selectively adsorbed on PS microstripes to reduce the interfacial energy of hydrophobic PS and PBLG blocks. This behavior essentially results from the strong interactions (such as hydrophobic interactions, and π–π interactions) between the hydrophobic PBLG blocks and PS microstripes. With the continuous addition of water, the adsorbed block copolymers self-assemble into nanostripes on the PS microstripes, and these nanostripes gradually undergo a structural reconstruction to further reduce the free energy of the system.[30,38] The PS microstripes act as confined surface to direct the self-assembly of PBLG-*b*-PEG block copolymers, and facilitate the formation of well-oriented nanostripes on PS microstripes with widths of 1.1–2.5 μm (Figure 1f–h). The confinement of PS microstripes not only promotes the formation of well-ordered nanopatterns, but also provides the prerequisite for the chirality expression of nanopatterns. Furthermore, the chiral sense of the nanopatterns in the present system mainly depends on the chirality of polypeptide blocks, which results from the chirality transmission process from polymers to nanopatterns.

In summary, we discovered the formation of chiral stripe nanopatterns through surface self-assembly of polypeptide-based rod-coil block copolymers on microstripes. The molecular chirality of the polypeptide blocks determines the chiral sense of nanopatterns. The chirality of the nanopatterns can be regulated by tuning the width of the PS microstripes as well as by mixing the $PBLG_{12k}$-*b*-PEG_{5k} and $PBDG_{12k}$-*b*-PEG_{5k} block copolymers. The information obtained from this work enriches our knowledge of the hierarchical chiral self-assembly of block copolymers containing helical segments, and may guide the design of 2D nanopatterns/nanostructures with tuned chiral features. Moreover, the resulting ordered chiral nanopatterns may find potential applications in bio-related fields.

Experimental Section

Polymer Synthesis: PBLG-*b*-PEG was synthesized in anhydrous 1, 4-dioxane solution using ring-opening polymerization of γ-benzyl-$_L$-glutamate-*N*-carboxyanhydride (BLG-NCA) initiated by anhydrous mPEG-NH_2 macroinitiator.[39] The reaction was performed in a flame-dried reaction bottle under a dry nitrogen atmosphere for 3 d at 15 °C. At the end of the polymerization, the reaction mixture was poured into a large volume of anhydrous ethanol. The precipitates were collected and dried under vacuum. The resulting products were purified twice by repeated precipitation from a chloroform solution into a large volume of anhydrous methanol. PBDG-*b*-PEG (PBDG: poly(γ-benzyl-$_D$-glutamate)) was synthesized using the same method. PBLG(FITC)-*b*-PEG copolymer was synthesized by partially replacing benzyl groups with fluorescein isothiocyanate (FITC). Details about the polymer synthesis are provided in Section S1.2 in the Supporting Information.

Preparation of the PS Microstripes: The PS microstripes on the substrate were prepared by using a controlled evaporative self-assembly method.[26,40,41] 10 μL of PS solution (M_n = 537 kg mol^{-1}, polymer concentration = 0.5 g L^{-1}) was trapped in a confined "cylinder-on-Si" geometry. As the solvent evaporated, regular PS microstripes were formed on the Si substrate. The obtained PS microstripes were then processed by heat treatment at ≈160 °C for 4 d followed by rinsing with large volumes of toluene ten times, leaving behind the ultrathin PS microstripes on the substrate.[28] Details about the preparation and characterization of the PS microstripes are available in Section S1.3 in the Supporting Information.

Preparation of the Stripe Nanopattern: For the self-assembly of PBLG-*b*-PEG on the PS microstripes, the copolymers were first dissolved in a THF/DMF mixture (7/3 v/v). The polymer concentration was 0.2 g L^{-1}, and the assembly temperature was 20 °C. Then, 3 mL of polymer solution was added to a beaker, and the substrate was immersed in solution with the PS microstripes facing up. To avoid solvent evaporation, the beaker was then sealed. Afterwards, 1.2 mL of water was added dropwise into the polymer solution by an injection pump. After self-assembly, the samples were rinsed with plenty of water to quickly remove the remaining organic solvent. Last, the samples were dried in vacuum for 12 h before further characterization.

Characterizations: The morphologies of the stripe nanopatterns were characterized by AFM and GISAXS measurements. AFM images were obtained with an XE-100 AFM instrument (Park Systems), employing noncontact mode. To gain clear images, the images were set by 256 × 256 pixels, and a scan rate of 0.5 Hz was employed. The images were analyzed using professional software (XEI, Park Systems). GISAXS experiments were performed at the Shanghai Synchrotron Radiation Facility (SSRF). The wavelength of the X-ray was 0.124 nm (E = 10 keV). For each sample, the incident angle was 0.3° and the exposure time was 100 s. The scattered intensity was collected by a detector (2048 × 2048 pixels, pixel size of 80 × 80 μm^2) placed at a distance of 1909 mm away from the sample. The CLSM image was captured by the Nikon A1R measurement. The signal of the fluorochromes was excited by an argon laser operating at 488 nm. The resulting outputs were obtained as digital false-color images.

Simulation Methods: Dissipative particle dynamics (DPD) simulation was used to study the structure of the stripe nanopatterns. In the DPD simulations, a volume of several molecules or parts of molecules were represented by a coarse-grained DPD bead. Corresponding to the molecular structure of the PBLG-*b*-PEG, a coarse-grained RC model consisting of a rod R block and a flexible C block was constructed. Neighbouring beads were connected via a harmonic spring force. In the DPD methods, all the units were scaled by the bead mass m, cut-off radius r_c and thermal energy k_BT. The equation of motion is integrated with a modified velocity Verlet algorithm with $\delta t = 0.04\tau$, where the time unit $\tau = (mr_c^2/k_BT)^{1/2}$. All the simulations were performed in an 80 × 80 × 40 simulation box, where the NVT ensemble and periodic boundary conditions were adopted. More than 2×10^7 DPD steps were performed so that the computing time was long enough for the system to achieve an equilibrium state. More details about the simulation parameter settings can be found in Section S2.2 in the Supporting Information).

Supporting Information

Supporting Information is available from the Wiley Online Library or from the author.

Acknowledgements

Z.T. and Z.X. contributed equally to this work. This work was supported by the National Natural Science Foundation of China (51833003, 51621002, 21975073, and 51573049).

Conflict of Interest

The authors declare no conflict of interest.

Keywords

rod-coil block copolymer, self-assembly, stripe nanopatterns, surface chirality, theoretical simulations

Received: June 30, 2020
Revised: August 9, 2020
Published online: August 23, 2020

[1] G. H. Wagnière, *On Chirality and the Universal Asymmetry: Reflections on Image and Mirror Image*, Wiley-VCH, Weinheim, Germany **2007**.
[2] R. M. Ho, Y. W. Chiang, S. C. Lin, C. K. Chen, *Prog. Polym. Sci.* **2011**, *36*, 376.
[3] M. Liu, L. Zhang, T. Wang, *Chem. Rev.* **2015**, *115*, 7304.
[4] E. Yashima, N. Ousaka, D. Taura, K. Shimomura, T. Ikai, K. Maeda, *Chem. Rev.* **2016**, *116*, 13752.
[5] Y. Fang, E. Ghijsens, O. Ivasenko, H. Cao, A. Noguchi, K. S. Mali, K. Tahara, Y. Tobe, S. De Feyter, *Nat. Chem.* **2016**, *8*, 711.
[6] X. Huang, C. Li, S. Jiang, X. Wang, B. Zhang, M. Liu, *J. Am. Chem. Soc.* **2004**, *126*, 1322.
[7] R. Fasel, M. Parschau, K. H. Ernst, *Nature* **2006**, *439*, 449.
[8] T. Chen, D. Wang, L. J. Wan, *Natl. Sci. Rev.* **2015**, *2*, 205.
[9] S. i. Sakurai, K. Okoshi, J. Kumaki, E. Yashima, *J. Am. Chem. Soc.* **2006**, *128*, 5650.
[10] F. Zaera, *Chem. Soc. Rev.* **2017**, *46*, 7374.
[11] M. Zhang, G. Qing, T. Sun, *Chem. Soc. Rev.* **2012**, *41*, 1972.
[12] G. Gao, M. Zhang, P. Lu, G. Guo, D. Wang, T. Sun, *Angew. Chem., Int. Ed.* **2015**, *54*, 2245.
[13] J. A. A. W. Elemans, I. De Cat, H. Xu, S. De Feyter, *Chem. Soc. Rev.* **2009**, *38*, 722.
[14] Y. Mai, A. Eisenberg, *Chem. Soc. Rev.* **2012**, *41*, 5969.
[15] I. W. Hamley, *Prog. Polym. Sci.* **2009**, *34*, 1161.
[16] C. Cai, J. Lin, T. Chen, X. S. Wang, S. Lin, *Chem. Commun.* **2009**, 2709.
[17] B. Yu, P. Sun, T. Chen, Q. Jin, D. Ding, B. Li, A. C. Shi, *Phys. Rev. Lett.* **2006**, *96*, 138306.
[18] Q. Zhang, J. Gu, L. Zhang, J. Lin, *Nanoscale* **2019**, *11*, 474.
[19] H. K. Choi, J. B. Chang, A. F. Hannon, J. K. W. Yang, K. K. Berggren, A. Alexander-Katz, C. A. Ross, *Nano Futures* **2017**, *1*, 015001.
[20] A. C. Shi, B. Li, *Soft Matter* **2013**, *9*, 1398.
[21] C. Cai, Y. Li, J. Lin, L. Wang, S. Lin, X. S. Wang, T. Jiang, *Angew. Chem., Int. Ed.* **2013**, *52*, 7732.
[22] C. D. Vacogne, C. Wei, K. Tauer, H. Schlaad, *J. Am. Chem. Soc.* **2018**, *140*, 11387.
[23] Y. Han, C. Cai, J. Lin, S. Gong, W. Xu, R. Hu, *Macromol. Rapid Commun.* **2018**, *39*, 1800080.
[24] S. Ji, L. Wan, C. C. Liu, P. F. Nealey, *Prog. Polym. Sci.* **2016**, *1*, 76.
[25] W. Li, M. Müller, *Prog. Polym. Sci.* **2016**, *54–55*, 47.
[26] W. Han, Z. Lin, *Angew. Chem., Int. Ed.* **2012**, *51*, 1534.
[27] M. Byun, W. Han, B. Li, X. Xin, Z. Lin, *Angew. Chem., Int. Ed.* **2013**, *52*, 1122.
[28] Y. Fujii, Z. Yang, J. Leach, H. Atarashi, K. Tanaka, O. K. C. Tsui, *Macromolecules* **2009**, *42*, 7418.
[29] N. Jiang, J. Shang, X. Di, M. K. Endoh, T. Koga, *Macromolecules* **2014**, *47*, 2682.
[30] W. Xu, Z. Xu, C. Cai, J. Lin, S. Zhang, L. Zhang, S. Lin, Y. Yao, H. Qi, *J. Phys. Chem. Lett.* **2019**, *10*, 6375.
[31] C. A. Fustin, N. Lefevre, R. Hoogenboom, U. S. Schubert, J. F. Gohy, *J. Colloid Interface Sci.* **2009**, *332*, 91.
[32] M. Lee, B. K. Cho, W. C. Zin, *Chem. Rev.* **2001**, *101*, 3869.
[33] J. Zhang, X. F. Chen, H. B. Wei, X. H. Wan, *Chem. Soc. Rev.* **2013**, *42*, 9127.
[34] J. F. Reuther, D. A. Siriwardane, R. Campos, B. M. Novak, *Macromolecules* **2015**, *48*, 6890.
[35] E. Yashima, K. Maeda, H. Iida, Y. Furusho, K. Nagai, *Chem. Rev.* **2009**, *109*, 6102.
[36] C. Harrison, D. H. Adamson, Z. Cheng, J. M. Sebastian, S. Sethuraman, D. A. Huse, R. A. Register, P. M. Chaikin, *Science* **2000**, *290*, 1558.
[37] M. H. Cativo, D. K. Kim, R. A. Riggleman, K. G. Yager, S. S. Nonnenmann, H. Chao, D. A. Bonnell, C. T. Black, C. R. Kagan, S. J. Park, *ACS Nano* **2014**, *8*, 12755.
[38] S. Zhang, C. Cai, Z. Guan, J. Lin, X. Zhu, *Chin. Chem. Lett.* **2017**, *28*, 839.
[39] C. Cai, L. Wang, J. Lin, X. Zhang, *Langmuir* **2012**, *28*, 4515.
[40] J. Xu, J. Xia, S. W. Hong, Z. Lin, F. Qiu, Y. Yang, *Phys. Rev. Lett.* **2006**, *96*, 066104.
[41] S. W. Hong, J. Xia, Z. Lin, *Adv. Mater.* **2007**, *19*, 1413.